

A numerical study on appearance of the runaway greenhouse state of a three-dimensional gray atmosphere

Masaki Ishiwatari¹

Division of Ocean and Atmospheric Sciences,
Graduate School of Environmental Earth Science, Hokkaido University, Sapporo, Japan

Shin-ichi Takehiro, Kensuke Nakajima

Department of Earth and Planetary Sciences,
Faculty of Sciences, Kyushu University, Fukuoka, Japan

Yoshi-Yuki Hayashi

Division of Earth and Planetary Sciences,
Graduate School of Science, Hokkaido University, Sapporo, Japan

Submitted to *J. Atmos. Sci* at 18 Jun. 2001,

Revised at 19 Apr. 2002 , accepted at 04 May 2002 ,

published at 15 Nov. 2002 (*J. Atmos. Sci.*, **59**, 3223–3238)

¹Corresponding author address: Dr. Masaki Ishiwatari, Division of Ocean and Atmospheric Sciences, Graduate School of Environmental Earth Science, Hokkaido University, 10 Kita 5 Nishi, Sapporo 060-0810, JAPAN. E-mail: momoko@ees.hokudai.ac.jp

Abstract

A numerical study on the runaway greenhouse state is performed by using a general circulation model (GCM) with simplified hydrologic and radiative processes. Except for the inclusion of three-dimensional atmospheric motion, the system utilized is basically equivalent to the one-dimensional radiative-convective equilibrium model of Nakajima *et al.* in which the runaway greenhouse state is defined.

The results of integrations with various values of solar constant show that there exists an upper limit of solar constant with which the atmosphere can reach a statistically equilibrium state. When the value of solar constant exceeds the limit, 1600 W m^{-2} , the atmosphere sets in a “thermally runaway” state. It is characterized by continuous increase of the amount of water vapor, continuous decrease of the outgoing longwave radiation, and continuous warming of the atmosphere and the ground surface.

The upper limit value of solar constant obtained by the GCM experiments corresponds to the upper limit of outgoing longwave radiation determined by the one-dimensional model of Nakajima *et al.* with a fixed value of relative humidity, 60 %, which is a typical value obtained by the GCM. The thermally runaway states realized in the GCM are caused by the radiation structure found by Nakajima *et al.* that prohibits the existence of thermal equilibrium states. The calculated values of upper limit of radiation and water vapor content cannot be directly applied to describing real planetary atmospheres, since the model physical processes are quite simple — gray radiation scheme without clouds. However, because of those simplification, our GCM gives deeper insight into the structure of a runaway atmosphere.

1 Introduction

The runaway greenhouse state is an important concept for understanding the variety of climates of the terrestrial planets. The previous studies using one-dimensional radiative-convective equilibrium models show that there exists an upper limit of outgoing longwave radiation (OLR) emitted from the top of the atmosphere on a planet with ocean. The nonequilibrium atmospheric state, which is expected to occur when the incident energy flux exceeds the limit value, is called the runaway greenhouse state (Nakajima *et al.* 1992, hereafter referred to as NHA92). In that state, it has been imagined that the atmospheric temperature will continue to rise until all of the oceans evaporate. Pollack (1971), using the one-dimensional radiative-convective equilibrium model for Venusian atmosphere, suggests the possibility that the proto-ocean of Venus disappears in its early history because of occurrence of a runaway greenhouse state. Abe and Matsui (1988) and Kasting (1988) argue that the runaway greenhouse state was realized on the growing proto-earth heated by the impacts of planetesimals and suggest emergence of a thick H₂O atmosphere and a magma ocean.

The structure of the atmosphere that causes the upper limit of OLR had not been thoroughly understood until the work of NHA92. Using a one-dimensional radiative-convective equilibrium model whose atmosphere is transparent to short-wave radiation and gray to longwave radiation, NHA92 clarifies that there are two different types of OLR limits. One is the limit constrained by the radiation flux going through the stratosphere. This limit is referred to as the Komabayashi-Ingersoll limit, since it is the key mechanism that causes runaway greenhouse states in the stratospheric models of Komabayashi (1967) and Ingersoll (1969). The other is the limit constrained by the emissivity of the troposphere. The runaway greenhouse states obtained by Pollack (1971), Abe and Matsui (1988) and Kasting (1988) are related to this type of limit. The limit of OLR that actually appears in a radiative-convective equilibrium model is the smaller of those two.

In this article, we consider occurrence of the runaway greenhouse state of a three-dimensional spherical atmosphere in the theoretical framework established by the one-dimensional model of NHA92. The issues to be focused on are the following problems which have been beyond the scope of one-dimensional radiative-convective equilibrium models. The first problem is nonuniform distribution of incoming solar radiation flux. As the incoming solar flux on the planet has a meridional distribution, it is not clear how the upper limit of OLR obtained by

one-dimensional models should be applied to the three-dimensional atmosphere.

The second problem is the effect of the atmospheric circulation. It is expected that the Hadley circulation dries the subtropical atmosphere. Consequently, a significant decrease of the subtropical optical depth is anticipated, and hence, the excess heat trapped in the equatorial region may be emitted from the subtropics (Pierrehumbert 1995). If the drying is intensified sufficiently, the upper limit of OLR will disappear and the runaway greenhouse state will not emerge.

The third problem is the dynamical behavior of the atmosphere near the steady solutions. As is explained in NHA92, one-dimensional radiative-convective equilibrium models give no information on the stability of the equilibrium solution of a system that includes water vapor feedback. The crucial assumption of one-dimensional radiative-convective equilibrium models of the NHA92 type is that the value of relative humidity is given as an external parameter. If this assumption is abandoned and humidity is predicted consistently in the system, there is the possibility that the steady states corresponding to the equilibrium solutions of NHA92 is unstable, for instance, in the sense of Plass (1961) and Gold (1964). The classical concept of the “runaway greenhouse” as stated by them is a dynamic instability resulting from a positive feedback loop; a warming of the surface results in an increase of the optical depth of the atmosphere that results in further warming of the surface.

The fourth problem is that the equilibrium models cannot describe inherently the atmospheric behaviors in the region where no steady state exists, that is, in the runaway greenhouse state. By the use of various cumulus parameterization schemes, Rennó *et al.* (1994) constructs time-dependent one-dimensional models, which enable us to have atmospheric states in the region where no steady state exists. It is shown that there exist solutions where the temperature increases continuously and a thermal equilibrium state cannot be achieved. However, the results are not analyzed in the theoretical framework of NHA92. It is not clear whether the “thermally runaway” state obtained by Rennó *et al.* (1994) corresponds to the realization of the runaway greenhouse state that should appear when the value of incoming solar flux exceeds the upper limit of radiation; their solutions might correspond to an unstable steady solution mentioned earlier in the third problem.

The model utilized in this study is a straightforward extension of the model of NHA92 to the three-dimensional time-dependent system. By this extension, we can examine whether the runaway greenhouse state can be defined for the three-

dimensional atmosphere in the framework of NHA92. As in NHA92, the details of the radiative processes, for example, the wavelength dependence of absorption coefficients, scattering, and the effects of clouds are not included. In this sense, the results of this paper cannot be applied immediately to the behavior of the real complex atmospheres. However, we expect that our findings about the atmospheric structure can serve as a useful framework for considering the complexity.

Section 2 explains the model, especially the methods that are necessary to make the long-term integration possible even when solar constant is increased. In Section 3, we will overview the results of the parameter study in which the value of solar constant is changed. It is shown that thermally runaway states occur in the three-dimensional system. In Section 4, we will examine the critical value of solar constant at which the thermally runaway state occurs. It is shown that the thermally runaway states obtained in three-dimensional calculations correspond to the runaway greenhouse state in the sense of NHA92. In Section 5, we will describe the change of the atmospheric structure associated with the increase of solar constant, focusing on the thermal structure and humidity field. In Section 6, conclusions and some discussions are presented.

2 Model and experimental design

2.1 Model

The system utilized is basically the same as that of the one-dimensional radiative-convective equilibrium model of NHA92, except for the inclusion of atmospheric three-dimensional spherical motion. The atmosphere consists of a condensable component and a noncondensable component; hereafter we refer to the former as water vapor and the latter as dry air, respectively. Both of these gases behave as ideal gases. We assume that specific heat and molecular weight of water vapor are the same as dry air so that those of the atmosphere are independent of the specific humidity (mass ratio of water vapor to entire air parcel). According to NHA92, this simplification does not alter the fundamental thermodynamical structure for the occurrence of the runaway greenhouse state. This assumption makes the density of model atmosphere smaller compared to the reality, and hence the intensity of circulation may be increased. Although the difference of density does not alter equations of motion in the σ coordinate (σ is the pressure divided by the

surface pressure), it causes some changes in energy equation. We have assumed that the difference of circulation intensity caused by this simplification is small and the dynamical structure of the system, for instance—existence of runaway state—if there is, does not change.

Only water vapor is assumed to absorb and emit longwave radiation, the absorption coefficient is constant and independent of wavelength. Dry air is assumed to be transparent; radiatively active noncondensable gases such as ozone or carbon dioxide are excluded. The radiative effects of clouds and the scattering of radiation are excluded, and hence all incident solar radiation reaches the ground surface. Those are the assumptions utilized in NHA92. The surface albedo can be set to zero. All of the planetary surface is assumed to be “swamp ocean” which is completely wet, has no heat capacity, and is always in heat balance. The values of the model parameters are listed in Table 1.

Parameters of model	Value
Molecular weight of dry air	$m_n = 18 \times 10^{-3} \text{ kg mol}^{-1}$
Molecular weight of water vapor	$m_v = 18 \times 10^{-3} \text{ kg mol}^{-1}$
Gas constant of dry air	$R_n = 461.9 \text{ J kg}^{-1}\text{K}^{-1}$
Gas constant of water vapor	$R_v = 461.9 \text{ J kg}^{-1}\text{K}^{-1}$
Specific heat at constant pressure of dry air	$c_{pn} = 3.5R = 1616.6 \text{ J kg}^{-1}\text{K}^{-1}$
Specific heat at constant pressure of water vapor	$c_{pv} = 3.5R = 1616.6 \text{ J kg}^{-1}\text{K}^{-1}$
Latent heat of water vapor	$L = 2.4253 \times 10^6 \text{ J kg}^{-1}$
Partial pressure of dry air at the bottom of atmosphere	$p_{n0} = 10^5 \text{ Pa}$
Absorption coefficient of water vapor	$\kappa_v = 0.01 \text{ m}^2\text{kg}^{-1}$
Absorption coefficient of dry air	$\kappa_n = 0 \text{ m}^2\text{kg}^{-1}$
Radius of planet	$a = 6.37 \times 10^6 \text{ m}$

Table 1: Values of the parameters used in the experiments.

Numerical experiments are performed by the use of GFD-Dennou-Club AGCM5 (SWAMP project, 1997) based on the three-dimensional primitive equation system on a sphere. The details of the model are described in Numaguti (1992). The equations are discretized horizontally by the use of nonalias latitude-longitude grid and integrated using the spectral method. The horizontal resolution utilized in the present study is 32×64 that corresponds to spectral truncation T21. We use σ as the vertical coordinate, which is discretized by following the method of Arakawa and Suarez (1983). The effect of convective clouds is parameterized by the moist convective adjustment scheme of Manabe *et al.* (1965). Turbulent diffusion is modeled by the level-2 closure scheme of Mellor and Yamada (1974). The surface fluxes of momentum, sensible heat, and latent heat are evaluated with bulk formulas, the bulk coefficients of which are evaluated by following Louis (1979).

The atmospheric structure expected to be realized in the runaway greenhouse state requires the following modifications of the model. First, the number of the vertical levels in the upper atmosphere should be increased. The tropopause must be allowed to reach a very high altitude level. Correspondingly, we specify that the uppermost vertical grid is located at $\sigma = 10^{-6}$ and the total number of levels is 32 (Table 2). This configuration of the model vertical levels ensures the accuracy of 5 W m^{-2} in the OLR calculation throughout the parameter range considered in NHA92. Secondly, the change of the total atmospheric mass must be taken into account. A significant increase of water vapor amount is anticipated in the states with an increased solar constant. The change of total atmospheric mass is evaluated with the surface pressure correction by the amount corresponding to the difference between the evaporation and precipitation. Details are given in Appendix A. For the same reason, we discard the approximation that the specific humidity is small, which is often employed in atmospheric models.

With those modifications summarized above, however, we have encountered a numerical instability problem in most of the experiments including the case with 1380 W m^{-2} as the value of solar constant. Close examination has revealed that the numerical instability is caused by the amplification of internal gravity waves in the uppermost region that is newly added to the model by the modification for the present study. For the 1380 W m^{-2} case, it has been possible to perform numerically stable long-term integrations, but with 16 vertical levels and $\sigma = 0.05$ as the top, as in the calculations of the previous studies (e.g., Numaguti, 1993; Horinouchi and Yoden, 1997; Akahori and Yoden, 1997; Hosaka *et al.*, 1998) where the original version of this model is used.

The extreme amplification of internal gravity waves is caused by the assumption that water vapor is the only radiatively active component. The typical value of the specific humidity obtained by the numerical calculations of the present study is $10^{-3} \sim 10^{-4}$ in the upper atmosphere. Based on this specific humidity and the absorption coefficient, the radiative relaxation time, with the radiation-to-space approximation, is estimated to be $300 \sim 3000$ days, which allows gravity waves excited in the lower atmosphere to propagate to the top of the model atmosphere almost without dissipation.

In this paper, instead of using a more sophisticated radiation scheme, we choose to introduce a strong artificial dissipation to suppress the internal gravity waves in the upper levels. We keep the simple radiation framework of NHA92 by reconciling the gravity wave representation. The artificial dissipation produces a

k	σ_k	$\sigma_{k+1/2}$
0		1
1	0.995	0.990
2	0.980	0.970
3	0.950	0.930
4	0.900	0.870
5	0.830	0.790
6	0.745	0.700
7	0.650	0.600
8	0.549	0.500
9	0.454	0.410
10	0.369	0.330
11	0.294	0.260
12	0.229	0.200
13	0.174	0.150
14	0.124	0.100
15	7.40×10^{-2}	5.00×10^{-2}
16	3.72×10^{-2}	2.54×10^{-2}
17	1.89×10^{-2}	1.29×10^{-2}
18	9.61×10^{-3}	6.58×10^{-3}
19	4.90×10^{-3}	3.34×10^{-3}
20	2.49×10^{-3}	1.70×10^{-3}
21	1.27×10^{-3}	8.65×10^{-4}
22	6.44×10^{-4}	4.40×10^{-4}
23	3.28×10^{-4}	2.24×10^{-4}
24	1.67×10^{-4}	1.14×10^{-4}
25	8.48×10^{-5}	5.78×10^{-5}
26	4.30×10^{-5}	2.94×10^{-5}
27	2.19×10^{-5}	1.50×10^{-5}
28	1.15×10^{-5}	7.60×10^{-6}
29	5.66×10^{-6}	3.87×10^{-6}
30	2.88×10^{-6}	1.97×10^{-6}
31	1.47×10^{-6}	1.00×10^{-6}
32	4.15×10^{-7}	0

Table 2: Position of the vertical grid points: k is the index of vertical level; σ_k and $\sigma_{k+1/2}$ indicate integer and semi-integer grids, respectively. Horizontal wind, temperature and specific humidity are evaluated at the integer grids, while vertical wind is evaluated at the semi-integer grids.

side effect in which the circulation structure in the upper levels are significantly altered. However, the basic structures of tropospheric circulation, such as Hadley cells and baroclinic waves, are represented (Section 5). We therefore believe that the degradation caused by the artificial dissipation is qualitatively not so serious as to distort the gross feature of the appearance of the runaway greenhouse state.

The artificial dissipation consists of Newtonian cooling, Rayleigh friction, and a vertical filter. The Newtonian cooling adjusts temperature T to its zonal mean value. The Rayleigh friction damps horizontal wind (u, v) toward 0. These are introduced to the seven levels from the top for all the experiments. Time constants of both the Newtonian cooling and the Rayleigh friction are set to be 10800 s at the uppermost level as in the Geophysical Fluid Dynamics Laboratory (GFDL) SKYHI model (Manzini and Hamilton, 1993). The time constants increase downwards; the value at the seventh level from the top is 75600 s. For the case with 1380 W m^{-2} of solar constant, the model can be integrated stably by introducing the Newtonian cooling and the Rayleigh friction only to the uppermost level as in the GFDL SKYHI model. However, for the experiments with increased solar constant, we have to introduce the linear dampings to the upper seven levels. In addition to the linear dampings, a vertical filter is introduced for T to suppress the growth of 2-grid noise. The detail of the vertical filter is described in appendix B. When the numerical instability still occurs, a vertical filter of Shapiro (1971) is adapted also for (u, v) .

2.2 Experimental design

As listed in Table 3, eight experiments are performed with different values of solar constant S . Each experiment is referred to as a letter S followed by the value of solar constant specified in the experiment. Experiment S1380 is the case corresponding to the present earth. Since all of the shortwave radiation is assumed to reach the ground surface, the global mean value of incoming shortwave radiation at the surface (SSR) is equal to $S/4$.

The distribution of incoming solar flux is given by the annual and daily average evaluated with the present terrestrial orbital parameters. The diurnal and seasonal cycles are not considered. The meridional distributions of the solar flux are shown in Fig. 1.

The initial condition is the same for all experiments. It is a resting, isother-

mal (280K) atmosphere with a constant specific humidity (10^{-3}). For each experiment, the model is integrated over 1000 days during which the atmosphere reaches a thermally equilibrium state, if it can.

Expt	Global mean SSR (W m^{-2})	Variables smoothed by vertical filter	Notes
S1200	300.0	T	○
S1380	345.0	T	○
S1500	375.0	T, u, v	○
S1550	387.5	T, u, v	○
S1570	392.5	T, u, v	○
S1600	400.0	T, u, v	×
S1700	425.0	T, u, v	×
S1800	450.0	T, u, v	×

Table 3: The list of experiments and the values of the solar constant. SSR is the shortwave radiation flux incident on the surface. White circles indicate the case where the model atmosphere reaches a thermally equilibrium state, while cross marks indicate the cases where it does not. For the details, see the description in Section 3.

3 Emergence of thermally runaway state

Let us examine first the dependencies of global mean surface temperature and global mean OLR on the value of the solar constant. The issue to be focused upon is whether there exists an upper limit of the solar constant value with which the three-dimensional atmosphere reaches a thermal equilibrium state. If an upper limit exists, its magnitude should be determined.

Fig. 2 shows the time evolution of global mean OLR and global mean surface temperature of experiments S1200, S1380, S1570 and S1800. As shown in Fig. 2a, for the cases with $S \leq 1570 \text{ W m}^{-2}$, the global mean OLR becomes equal to the global mean SSR, which is equal to $S/4$, in about 500 days, and the atmospheric system reaches a statistically steady state. The global mean surface temperature also settles down to an equilibrium value (Fig. 2b).

In the experiment S1800, on the other hand, the system goes into a thermally runaway state. The global mean surface temperature keeps increasing (dashed-dotted line in Fig. 2b). The atmosphere emits infrared radiation less than the

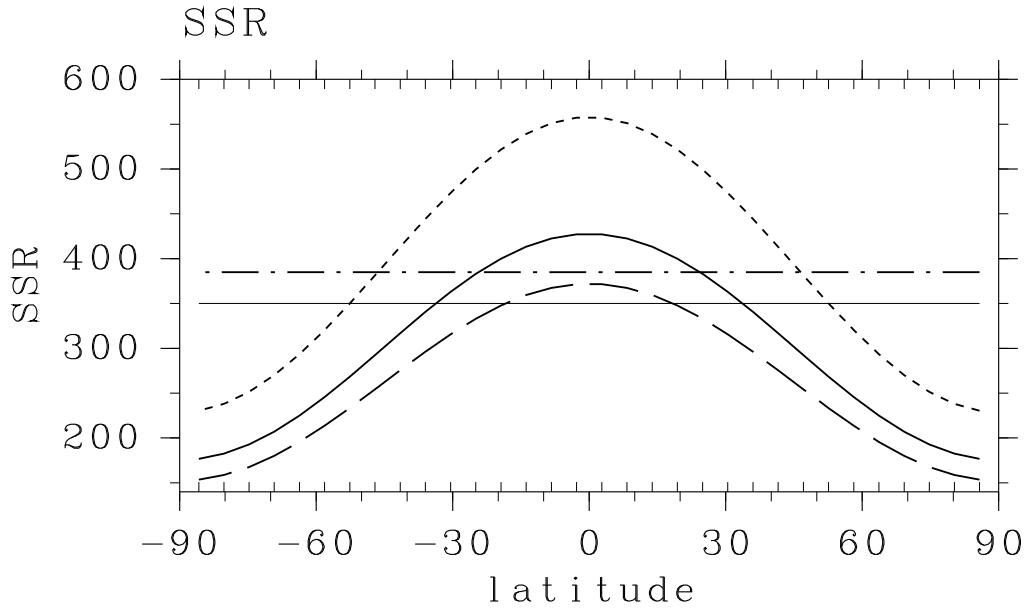


Figure 1: Meridional distributions of incident solar radiation flux. Unit is W m^{-2} . Thick solid line, dashed line and dotted line are for $S = 1380 \text{ W m}^{-2}$, $S = 1200 \text{ W m}^{-2}$ and $S = 1800 \text{ W m}^{-2}$, respectively. Dotted-dashed line indicates the Komabayashi-Ingersoll limit (385.2 W m^{-2}), and thin solid line indicates the upper-limit value of OLR (355.0 W m^{-2}) obtained by the NHA92 model. Both of them are calculated with the parameters of the present study.

incoming total solar flux, since the calculated value of global mean OLR is always less than 450 W m^{-2} (dashed-dotted line in Fig. 2a). Moreover, the global mean OLR decreases gradually as time goes on, and hence, the excess in the energy budget, that is, the difference between the given SSR and the global mean OLR, increases. The atmospheric system does not seem to approach any thermal equilibrium states.

Fig. 3 summarizes the relationship between the externally given global mean SSR and the global mean OLR obtained at the end of the time integration for all of the experiments. When $S < 1600 \text{ W m}^{-2}$, that is, the global mean SSR is less than 400 W m^{-2} , the global mean OLR almost exactly equals the global mean SSR, and the atmosphere reaches an equilibrium state. On the other hand, when $S \geq 1600 \text{ W m}^{-2}$, that is, the global mean SSR is 400 W m^{-2} or larger, the atmosphere cannot reach an equilibrium state. All of the results obtained with $S \geq 1600 \text{ W m}^{-2}$ are thermally runaway states characterized by continuous decrease of OLR and continuous increase of surface temperature, as is shown for the case of S1800 in Fig. 2.

It is now confirmed that there exists an upper limit on the value of solar constant with which the three-dimensionally circulating atmosphere reaches a thermal equilibrium state. The value of the upper limit is about 1600 W m^{-2} , or 400 W m^{-2} as global mean SSR, in our configuration. In the following sections, we will examine the correspondence of the thermally runaway states obtained by the three-dimensional calculations with the runaway greenhouse state defined by the one-dimensional model of NHA92. An interpretation of the upper-limit value of the solar constant will also be given.

4 Comparison with one-dimension system

Fig. 4 shows the meridional distributions of zonal mean OLR and zonal mean surface temperature for the cases with $S \leq 1570 \text{ W m}^{-2}$ where the atmosphere can reach a thermal equilibrium state. As the incident solar flux increases, the meridional distribution of OLR is flattened and the value of OLR approaches about 400 W m^{-2} at all latitudes. The value of OLR in the equatorial region ceases to increase at around 390 W m^{-2} when $S = 1500 \text{ W m}^{-2}$ and the value hardly changes against the further increase of solar constant. In the mid- and high latitudes, the value of OLR gradually approaches 400 W m^{-2} with the increase of

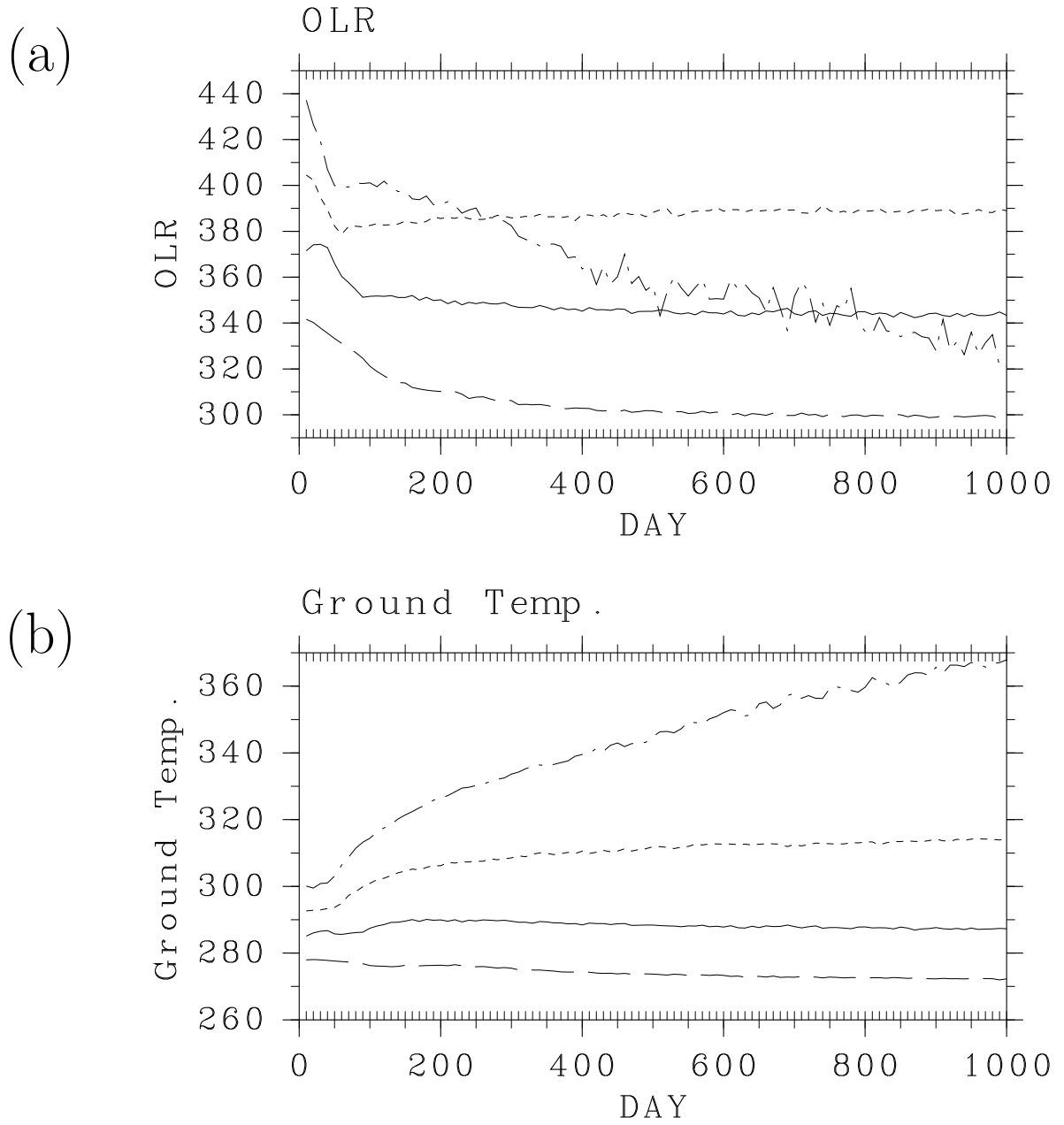


Figure 2: Time evolutions of (a) global mean OLR (W m^{-2}) and (b) global mean surface temperature (K). Dashed line, solid line, dotted line and dashed-dotted line indicate experiments S1200, S1380, S1570 and S1800, respectively.

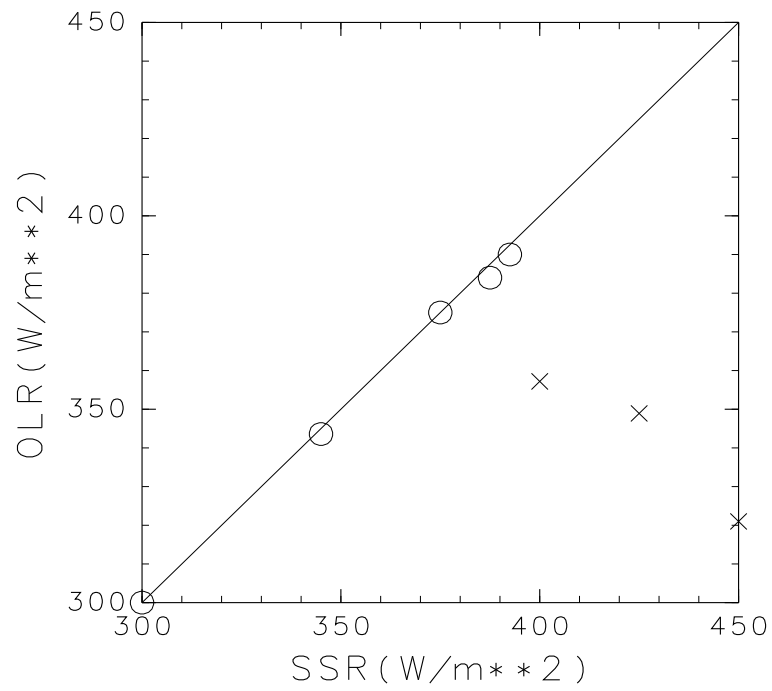


Figure 3: The relationship between global mean SSR and global mean OLR. The values of OLR at day 1000 are plotted except for S1600 where the value is at day 2000. White circles represent the cases where the atmosphere reaches an equilibrium state, while cross marks represent the cases where the atmosphere is in a thermally runaway state. Note that the values of OLR for thermally runaway states are continuously decreasing.

the solar constant. The tendency similar to that of OLR distribution appears in the meridional distribution of zonal mean surface temperature.

The asymptotic value of OLR is close to the value of the Komabayashi-Ingersoll limit, 385 W m^{-2} . However, the existence of asymptote of OLR does not result from the existence of the Komabayashi-Ingersoll limit. An OLR value of 385 W m^{-2} is the Komabayashi-Ingersoll limit obtained by the use of the one-dimensional model of NHA92 in which the atmosphere is assumed to be saturated at the tropopause. We should examine the stratospheric water vapor content in order to compare the asymptotic value of OLR with the Komabayashi-Ingersoll limit. In experiment S1570, the value of stratospheric relative humidity is only about 50% (Fig. 9d). For this value of relative humidity, the Komabayashi-Ingersoll limit is 450 W m^{-2} . This value is larger than the asymptotic value of OLR obtained in the three-dimensional calculations.

The asymptotic value of OLR is actually close to the upper limit of radiation which is constrained by the tropospheric temperature structure as discussed in NHA92. In order to apply the discussion by NHA92, it is necessary to examine the value of tropospheric relative humidity. In experiment S1570, the averaged value of relative humidity in the equatorial troposphere is about 60 % (Fig. 9d). The upper limit of radiation obtained by the one-dimensional radiative-convective equilibrium model is 385 W m^{-2} when the value of relative humidity for the radiation scheme is fixed to be 60 %. This value is close to 390 W m^{-2} , the equatorial value of OLR obtained in our three-dimensional calculations.

Now, we will compare the tropospheric temperature structures of the three-dimensional results with those of one-dimensional equilibrium solutions to examine whether there exists a tendency of the temperature field to approach an asymptotic profile as a function of optical depth as discussed by NHA92. Fig. 5 shows the temperature structures obtained by the one-dimensional radiative-convective equilibrium model in which relative humidity is fixed to be 60%. In Fig. 5a, where the temperature is plotted as a function of pressure, the asymptotic feature is not obvious; as surface temperature increases, the entire vertical profile is simply shifted to the positive direction of the temperature axis. However, in Fig. 5b, where the temperature is plotted as a function of optical depth, the temperature structures closely approach the curve determined by the saturation water vapor pressure. Especially, for the cases corresponding to S1600, S1700, S1800, the profiles almost coincide with each other. NHA92 pointed out that the existence of this asymptote is the essential feature for the appearance of runaway greenhouse

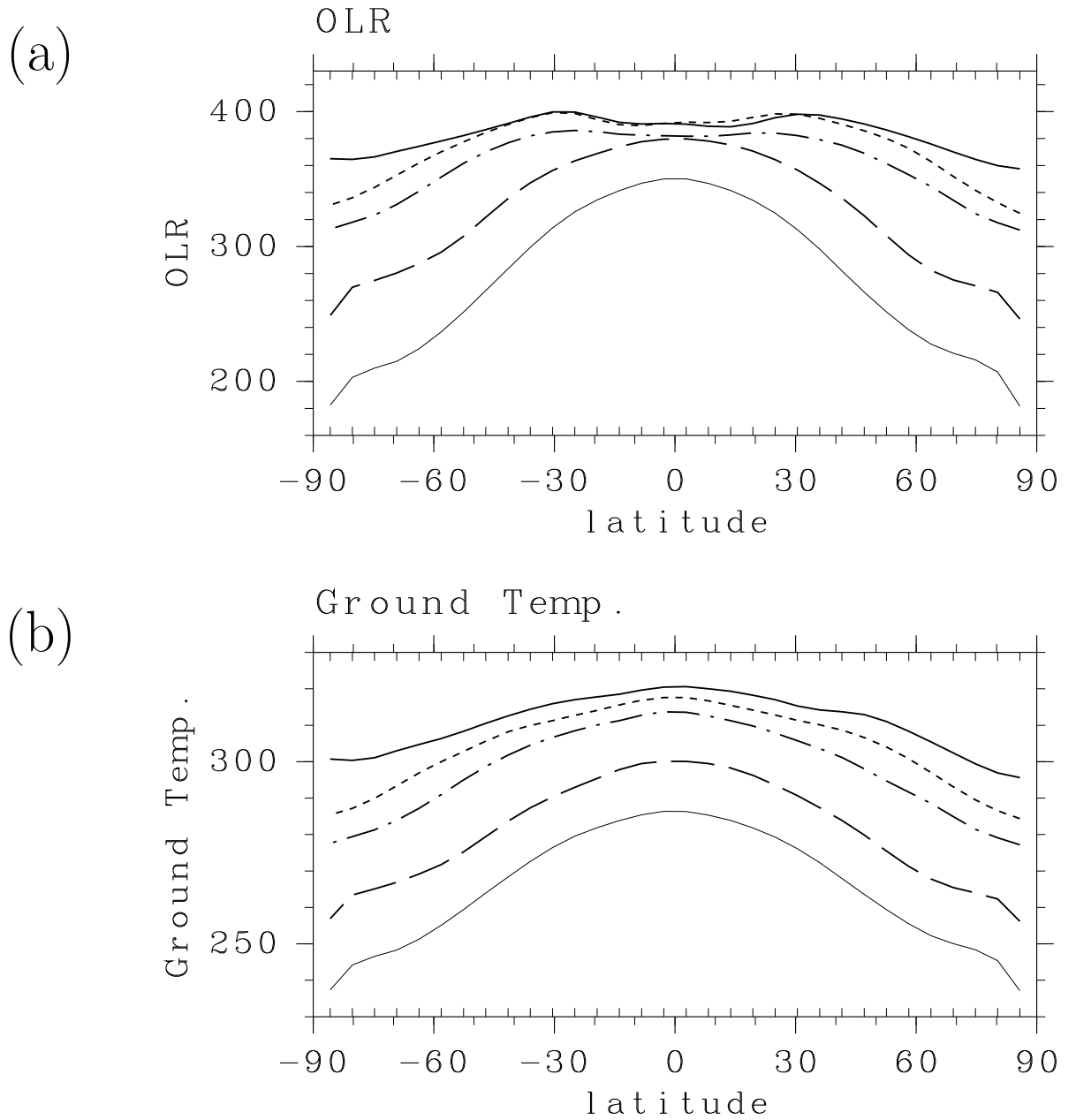


Figure 4: The meridional distributions of (a) zonal mean OLR (W m^{-2}) and (b) zonal mean surface temperature (K) of the cases in which the system reaches equilibrium states. Thick solid line, dotted line, dotted-dashed line, dashed line, and thin solid line indicate experiments S1570, S1550, S1500, S1380, and S1200, respectively. The data are temporally averaged between days 950 and 1000.

state in the one-dimensional equilibrium model.

As for the three-dimensional results, the tropospheric temperature profiles as a function of optical depth τ also seem to have an asymptote (Fig. 6b), while the profiles as a function of pressure scatter just as one-dimensional equilibrium solutions (Fig. 6a). The existence of an asymptote can be observed in the deep troposphere of the thermally runaway states (experiments S1600, S1700, S1800), where $\tau \gg 1$. This is because the specific humidity there is fairly large as to ensure that temperature gradient almost coincides with that of the saturation vapor pressure curve. In the upper troposphere, where the value of τ is smaller, the results of the three-dimensional calculations show a less clear asymptotic feature compared to those of one-dimensional equilibrium model. The reasons are that the mean temperature structures obtained by explicit calculations of the atmospheric circulation do not precisely coincide with the moist adiabatic structure and that the value of relative humidity changes with the value of solar constant. The deviation of temperature from the moist adiabatic structure is caused by the fact that there are regions of the atmosphere in which the temperature gradient is steeper than the moist adiabatic gradient, but humidity is not large enough to trigger moist convection because of lateral mixing between the equator and mid-latitude. In the stratosphere, the temperature obtained by the three-dimensional calculations (Fig. 6) varies almost randomly. It seems that the large-amplitude gravity waves, as described in Section 2, contribute to the stochastic deviation of the stratospheric temperature from the equilibrium solution. Moreover, with the calculated values of humidity, the stratospheric radiative relaxation time of these experiments is very long. For instance, in the equilibrium state of experiment S1570, stratospheric specific humidity is 10^{-4} for which the estimated relaxation time is about 3000 days. Random appearance of stratospheric temperature is, therefore, inevitable in the 50-day mean profiles. Unless OLR exceeds the Komabayashi-Ingersoll limit, the random variation of temperature in the upper atmosphere is not important for the determination of the upper limit of radiation, because the region where temperature varies randomly is optically thin.

Fig. 7 shows the relationship between surface temperature and OLR obtained by the one-dimensional calculation similar to those given by NHA92 except that the value of relative humidity for the radiation calculation is varied between 40% and 100%. In Fig. 7, the points representing the equatorial zonal mean values of surface temperature and OLR obtained by the three-dimensional calculations are also plotted. The surface temperature–OLR relationship obtained by three-dimensional calculation is well correlated with the curve of the one-dimensional model with 60%

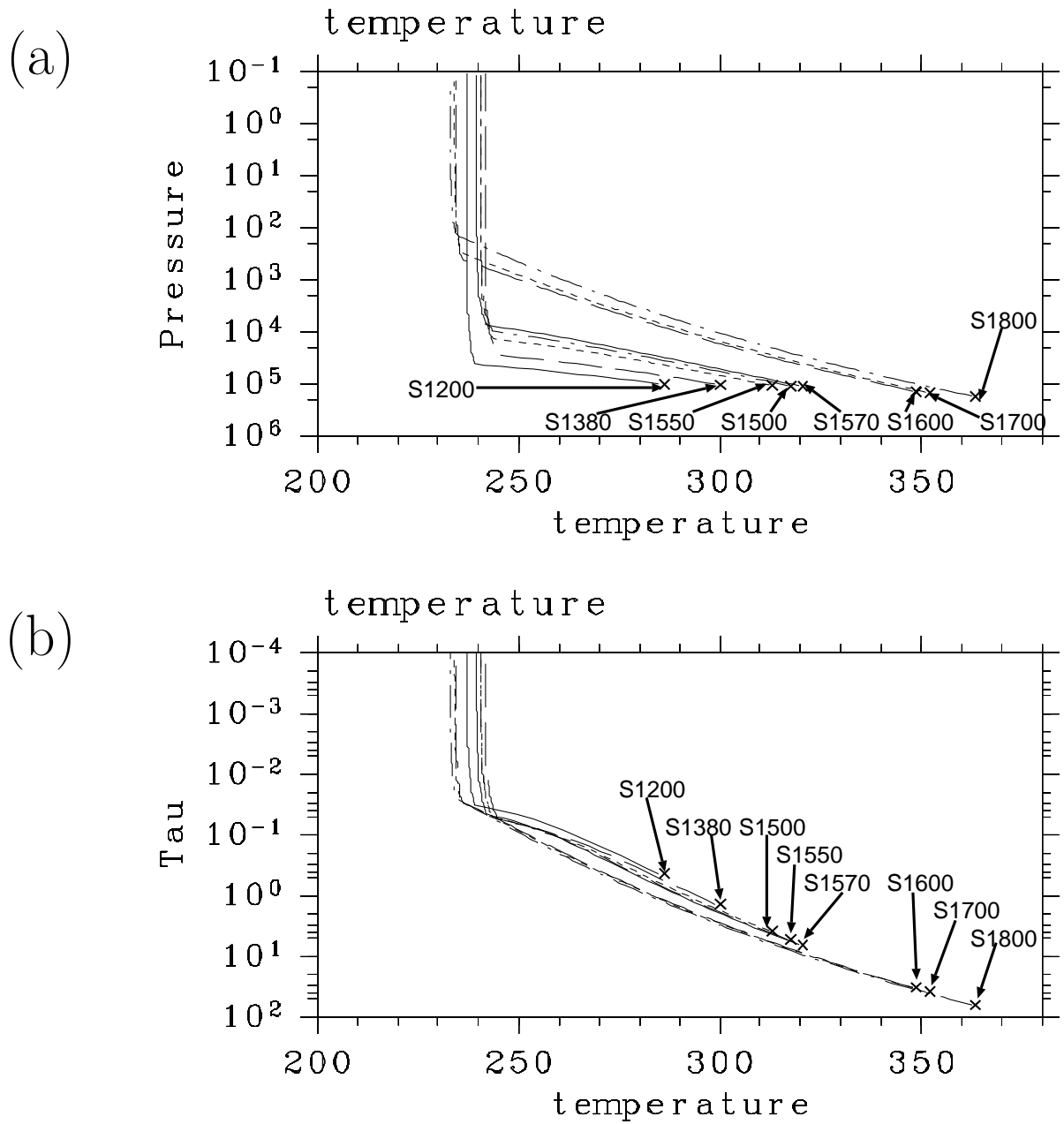


Figure 5: Vertical distributions of temperature obtained by one-dimensional model with relative humidity of 60 % for the radiation scheme. The profiles are plotted by specifying the values of temperature at the bottom of atmosphere as those obtained by the experiments. Ordinates are (a) pressure (Pa) and (b) optical depth. Cross marks indicate surface temperature.

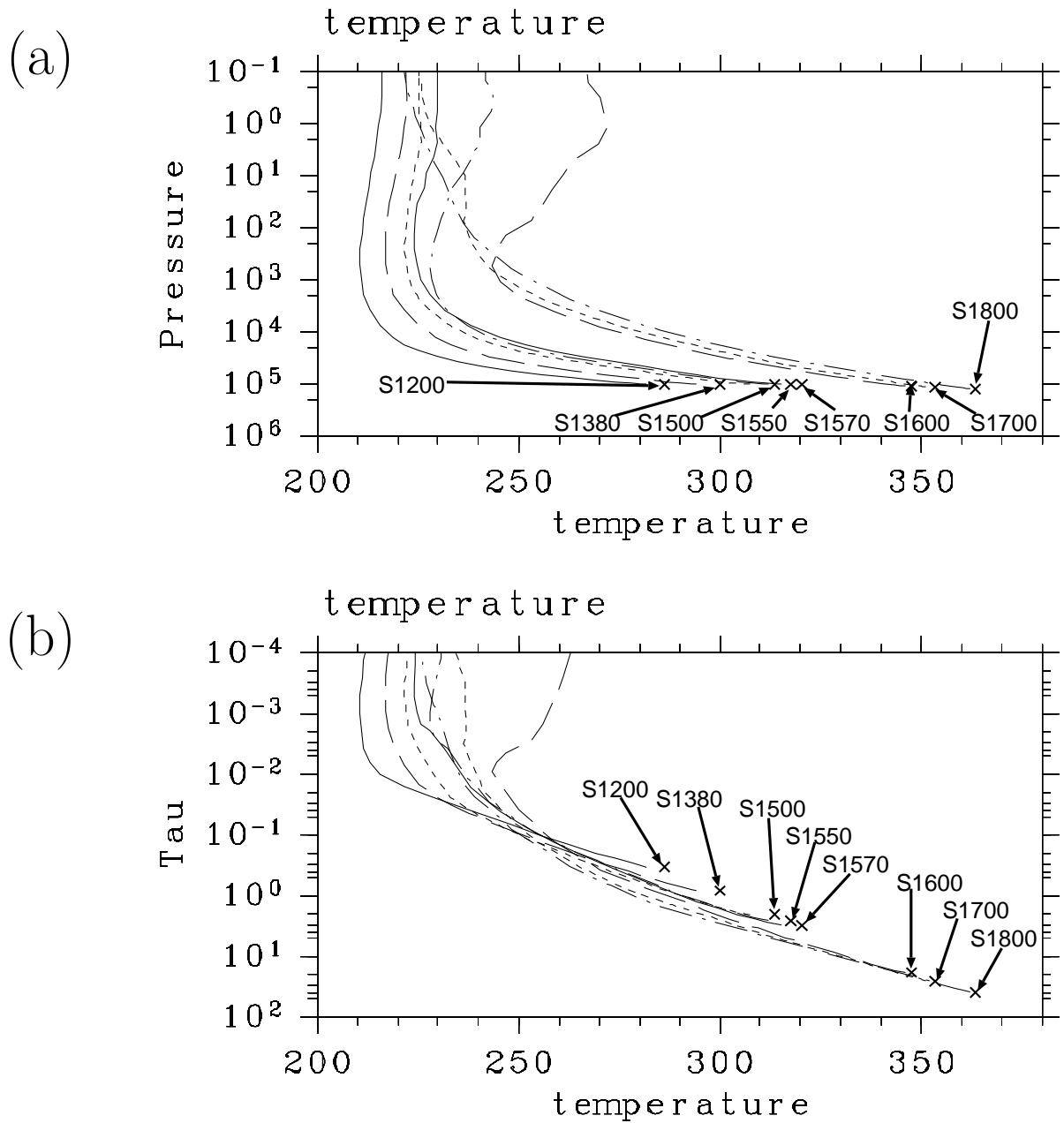


Figure 6: Vertical distributions of zonally averaged temperature at the equator for various values of solar constant. Ordinates are (a) pressure (Pa) and (b) optical depth. The profiles obtained in the experiments S1800, S1700, S1600, S1570, S1550, S1500, S1380, S1200 are plotted. Cross marks indicate surface temperature.

relative humidity. There exists a slight difference. The causes of the difference are that the value of tropospheric relative humidity is larger than 60% in experiments S1200 ~ S1500 and that the temperature gap between the surface and the lowest level of the model, which is allowed in the three-dimensional model but not in one-dimensional calculations, becomes significant in experiments S1550 and S1570. In thermally runaway states (S1600, S1700, S1800), OLR decreases as the solar constant increases, since the relative humidity in the upper troposphere increases (not presented here).

As a result of the above discussion, it can be concluded that the asymptotic value of OLR obtained by three-dimensional calculations corresponds to the upper limit of radiation of the one-dimensional radiative-convective equilibrium solution in which the value of relative humidity is taken into account. The existence of the upper limit of OLR in the three-dimensional system means that the runaway greenhouse state can be defined also in three-dimensional system as the state realized when the incident radiation exceeds the upper limit of OLR, that is, the runaway greenhouse state defined by NHA92. It is considered that the thermally runaway states obtained in experiments S1600, S1700 and S1800 correspond to the runaway greenhouse state.

The condition for the occurrence of runaway greenhouse state in the three-dimensional system is that the global mean value of incident flux exceeds the upper limit of OLR; neither the maximum nor minimum of the latitudinal distribution of incident flux is relevant to the condition for the configuration of the present work. When the incident radiation is increased, the equatorial OLR reaches the upper limit and cannot be increased any more. When the incident radiation is further increased, the heat excess in the Tropics is transported to the higher latitudes as described in the next section, and OLR in the mid- and high latitudes increases until it reaches the upper limit. In other words, the runaway greenhouse state does not appear until OLR runs up to the upper limit globally. For SSR whose global mean value is below the limit, a three-dimensional statistically equilibrium solution, which corresponds to solution on the branch with increasing OLR against surface temperature in Fig. 7, exists and is dynamically stable.

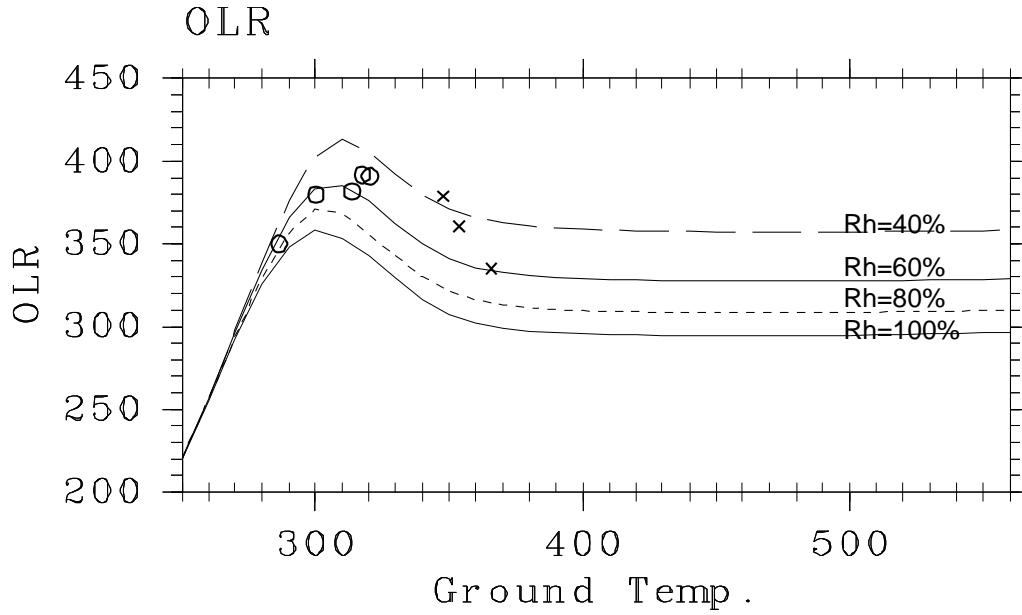


Figure 7: The relationship between surface temperature (K) and OLR (W m^{-2}). Curves represent surface temperature–OLR relationship obtained by the one-dimensional radiative-convective equilibrium model with various values of relative humidity for the radiation scheme. Thin solid line, dotted line, thick solid line and dashed line indicate 100 % of relative humidity (the same as the results of NHA92), 80 %, 60 % and 40 %, respectively. Marks represent the relationship between equatorial zonal mean values of surface temperature and OLR obtained by GCM. White circles and cross marks represent the results where the system reaches an equilibrium state and where the system cannot, respectively.

5 Circulation structure toward the runaway greenhouse state

In this section, we will observe the change of meridional circulation fields with the increase of solar constant to examine how the latitudinally uniform distribution of OLR becomes established and why the subtropical region is not fully dried. According to our results, the subtropical drying does appear; a careful observation of Fig. 4 shows that, in the cases with $S \geq 1500 \text{ W m}^{-2}$, the subtropical values of OLR are slightly greater than those at the equator. However, the subtropical drying does not proceed to such an extent as imagined in Section 1 so that the occurrence of a runaway greenhouse state is not prevented.

Figures 8, 9, and 10 show the zonal mean meridional circulation structures of the experiments S1380, S1570 and S1800, respectively. The plotted data are averaged for 50 days. In the experiment S1800, the temporal variation is so large that even for the zonal mean fields, 50 day is not enough to smooth out the variation. However, we cannot adapt the longer period for averaging, since the model atmosphere of the experiment S1800 is in the runaway greenhouse state and its circulation fields are secularly changing. The plotted period for S1800 is selected as the duration when the Hadley circulation shows relatively clear symmetry around the equator.

With the increase of incoming solar flux, the intensity and height of the Hadley circulation increases (Figs. 8e, 9e, 10e). Corresponding to this change, the amount of equatorial precipitation increases and the peak of heating profile is shifted upward (Figs. 8b, 9b, 10b). It is noteworthy that the downward branch of Hadley cells remains at around $\pm 30^\circ$. The latitudinal width of Hadley cells hardly changes with the change of solar flux, which is consistent with the theory of Satoh (1994).

Subtropical drying appears for all the experiments in the sense that the values of relative humidity in the subtropics are less than those of the equatorial region. However, associated with the intensification of the Hadley circulation, the equatorial relative humidity also decreases, and hence, the difference between the subtropical and equatorial values of relative humidity decreases (Figs. 8d, 9d, 10d).¹ Relative humidity of the whole Tropics decreases with the increase

¹The values of specific humidity and relative humidity of the experiment S1380 are large compared to those of the real terrestrial atmosphere. This is not caused by the simplicity of the

of the solar constant, but its value does not become extremely small. Even for the experiment S1800, the value of relative humidity in the subtropics is not less than 30%. Consequently, as is evident from the specific humidity fields (Figs. 8c, 9c, 10c), the absolute amount of water vapor increases steadily in all region including subtropics. The increase of humidity in subtropical region is caused by the increased moisture transport by eddies (Fig. 14), as will be discussed later. The atmosphere becomes optically thick with the increase of incoming solar radiation as shown in the meridional distributions of optical depth (Fig. 11).

As for the temperature fields, the meridional difference of temperature decreases as the solar flux increases (Figs. 8a, 9a). In the runaway greenhouse state (Fig. 10a), the meridional difference of temperature almost disappears, which corresponds to the disappearance of meridional contrast of OLR profile. In the equilibrium states (S1570), however, detailed examination of Fig. 9a shows that subtropical temperature is significantly lower than that of equator, although the meridional contrast of OLR is fairly small (Fig. 4a). This is because the changes of latitudinal profiles of temperature and humidity with the increase of solar flux have opposite effects on the change of subtropical OLR; cold subtropics cause OLR to be smaller, while dry subtropics cause OLR to be larger.

The results of this compensation can be observed in Fig. 12, which shows the meridional structure of temperature with optical depth as the vertical coordinate. For the experiment S1570, whose solar constant is just below the value for entering the runaway greenhouse state, the water vapor amount in the subtropical regions is relatively smaller than that of the equatorial region, and hence the $\tau = 1$ surface in the subtropical regions is located at the lower altitude (Fig. 11b). On the other hand, the temperature profile has its maximum at the equator and decreases toward both poles (Fig. 9a). Consequently, the temperature profile on the surface of $\tau = 1$ is more uniform than that on the surface of constant σ (Fig. 12b). The latitudinal profile of OLR tends to be flat even in the experiments whose solar constant is below runaway value, although there still exists a significant amount of latitudinal temperature difference. In those ways, the values of OLR at all latitudes gradually approach the equatorial limit as the value of solar constant is

present model. Actually, the value of the experiment S1380 are also large compared to a series of previous studies with the same model [(e.g., Numaguti 1993; Horinouchi and Yoden 1997; Akahori and Yoden 1997; Hosaka *et al.* 1998). Zonal mean distributions of specific humidity and relative humidity, for instance, are shown in Hayashi *et al.* 2000]. The difference between the present model and previous ones is that the present model utilizes gray radiation scheme, while others utilizes a four-band radiation scheme. Gray radiation makes the height of Hadley circulation lower. We speculate that the decrease of tropospheric height weakens the effect of cold trap and increases the amount of humidity.

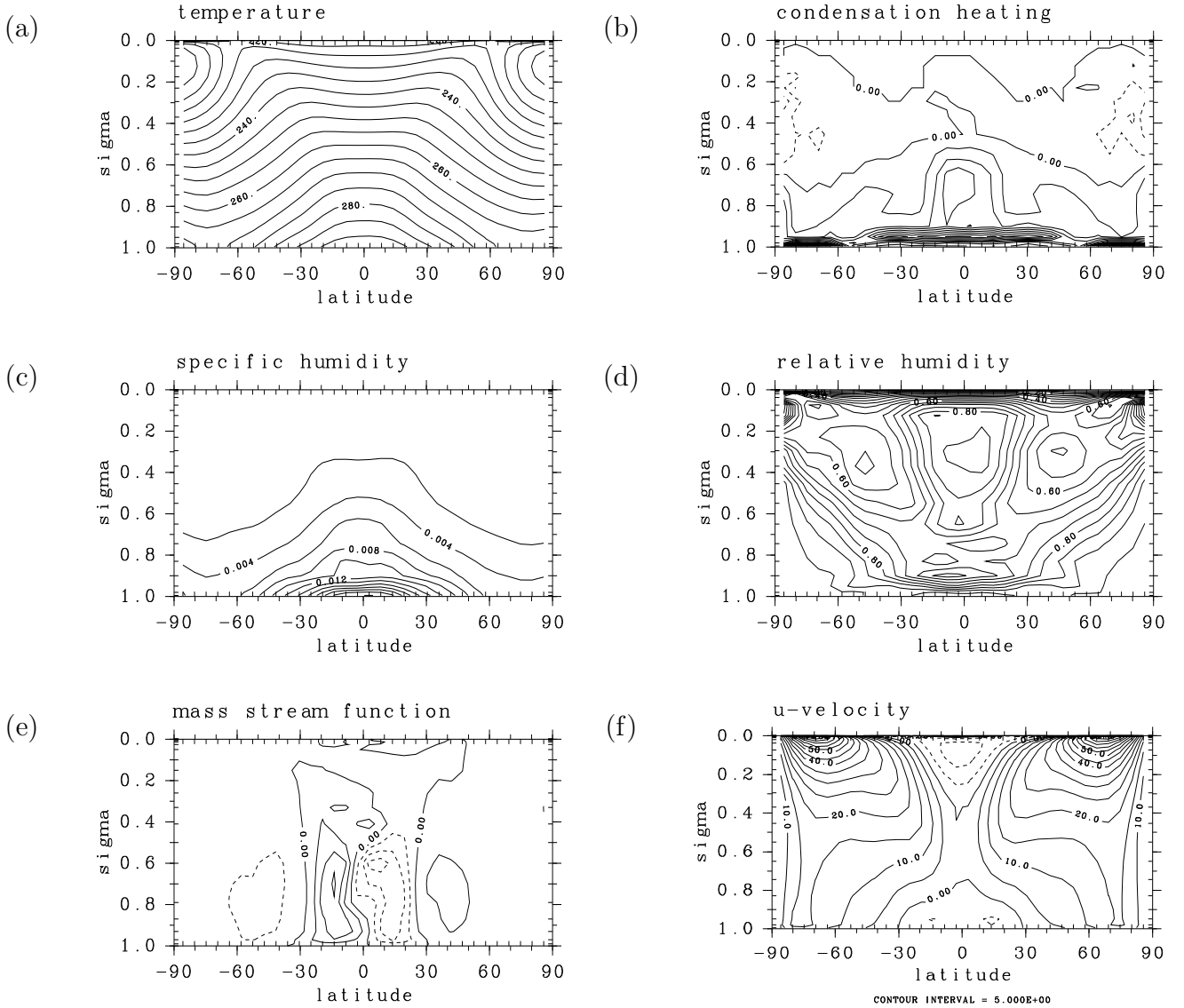


Figure 8: Meridional structures of the zonal mean circulation fields of the experiment S1380: (a) temperature, (b) condensation heating, (c) specific humidity, (d) relative humidity, (e) mass stream function, and (f) zonal wind. Contour intervals are (a) 5 K, (b) 5×10^{-6} K day $^{-1}$, (c) 2.0×10^{-3} , (d) 0.05, (e) 5 m s $^{-1}$, (f) 1.0×10^{10} kg s $^{-1}$, respectively. Time mean fields between $t = 950$ to 1000 days are plotted.

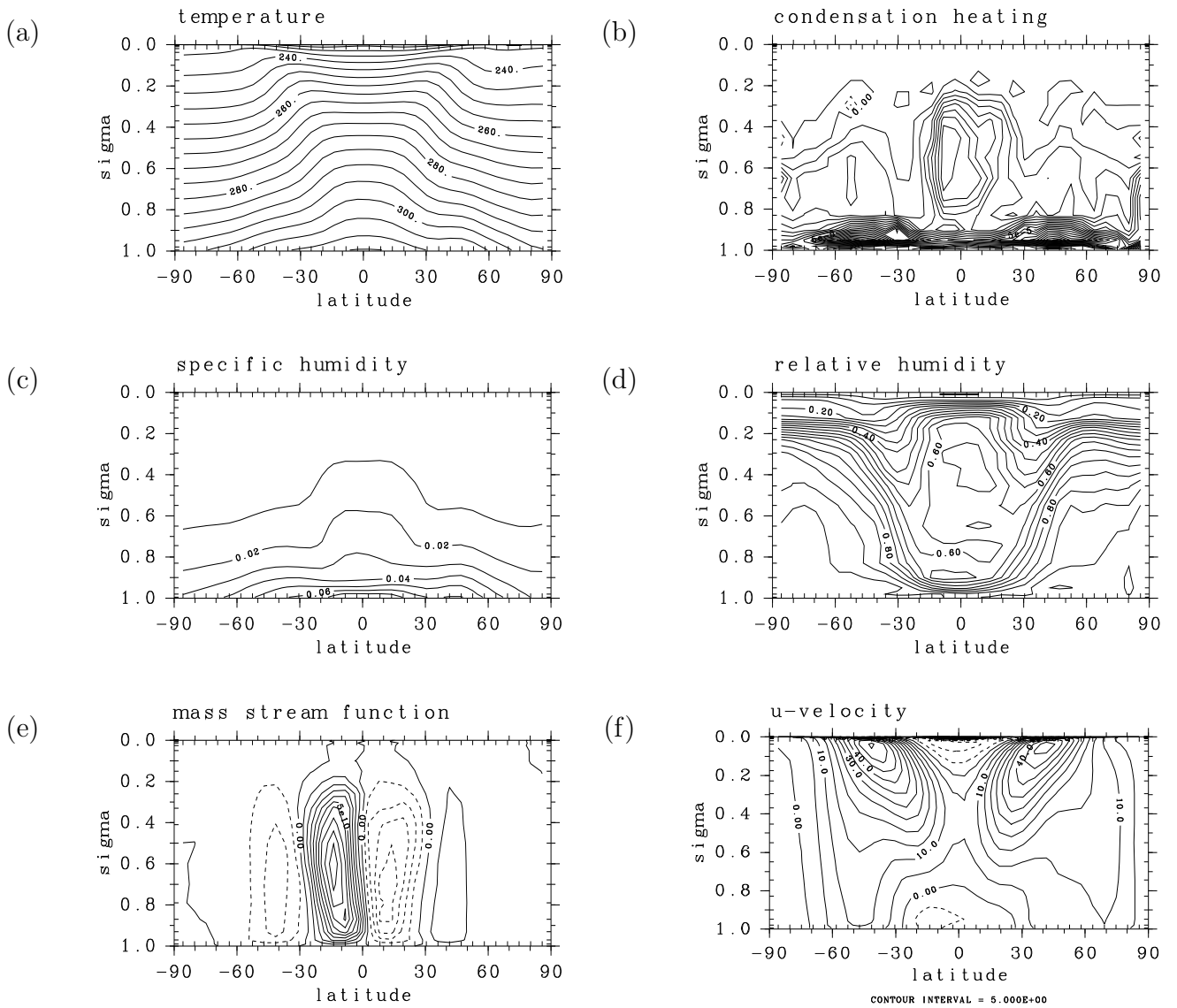


Figure 9: Same as in Fig. 8 but for the experiment S1570. Contour intervals are the same as in Fig. 8 except for (c) 1.0×10^{-2} .

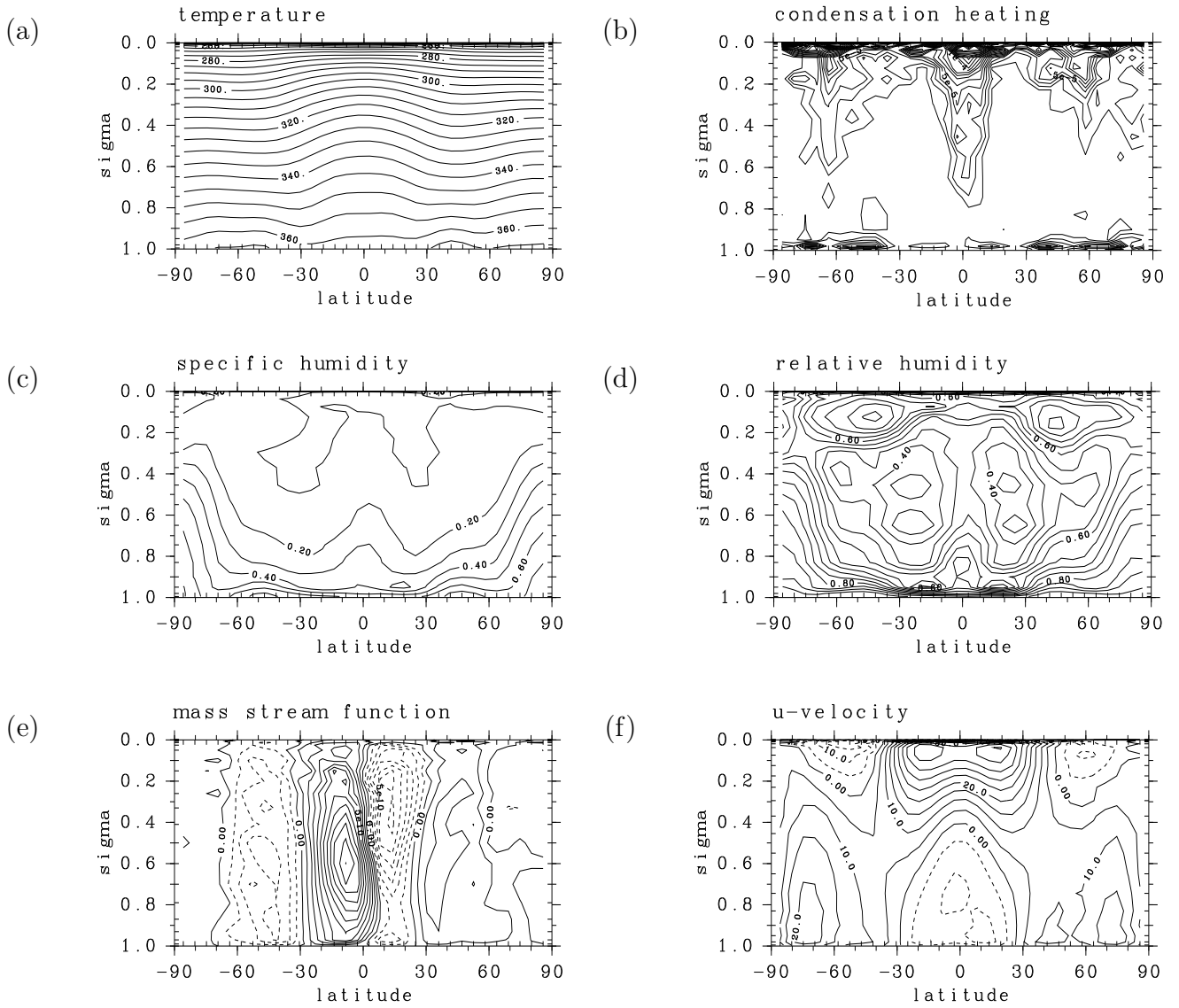


Figure 10: Same as in Fig. 8 but for the experiment S1800. Time-mean fields between $t = 870$ to 920 days are plotted. Contour intervals are the same as in Fig. 8 except for (b) $1 \times 10^{-5} \text{ K day}^{-1}$ and (c) 0.1.

increased toward this limit.

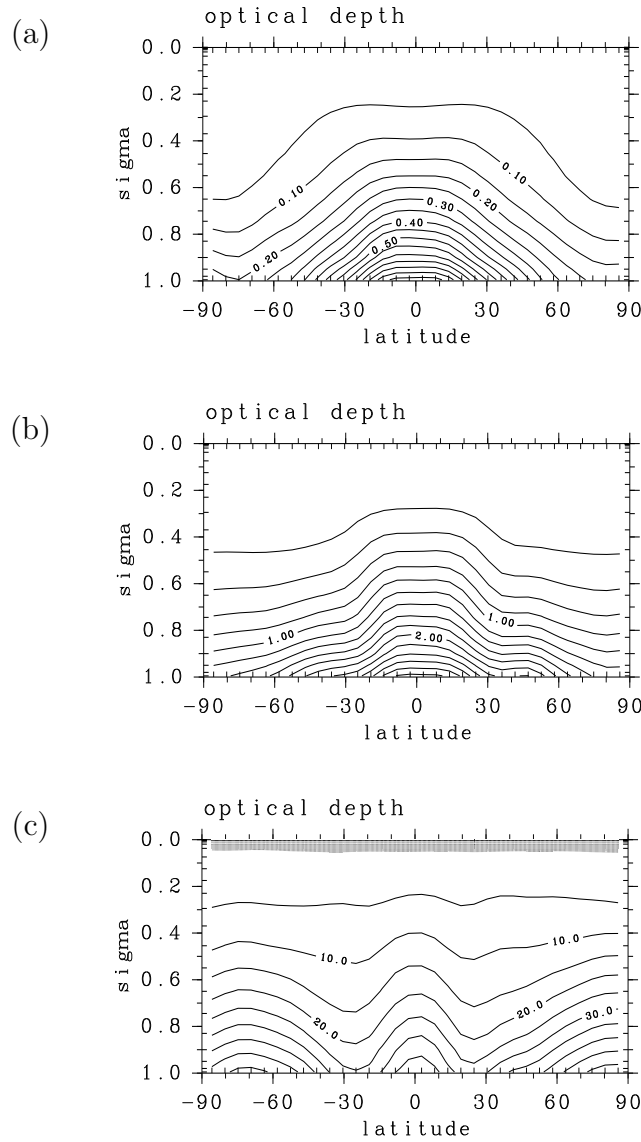


Figure 11: Meridional structure of zonal mean optical depth in the experiments (a) S1380, (b) S1570, and (c) S1800. Here, σ is used as the vertical coordinate. The contour intervals are (a) 0.05, (b) 0.2, and (c) 5.0, respectively. The shaded areas in (c) represent the area with optical depth less than 1.

There should be an increase of poleward heat transport to have a latitudinally uniform OLR distribution, since the latitudinal gradient of incoming heat supply increases as solar constant increases. This actually is achieved by the increase of latent heat flux. Fig. 13 shows the latitudinal distributions of heat fluxes. With the increase of solar constant, latent heat flux dominates radiation flux in the surface

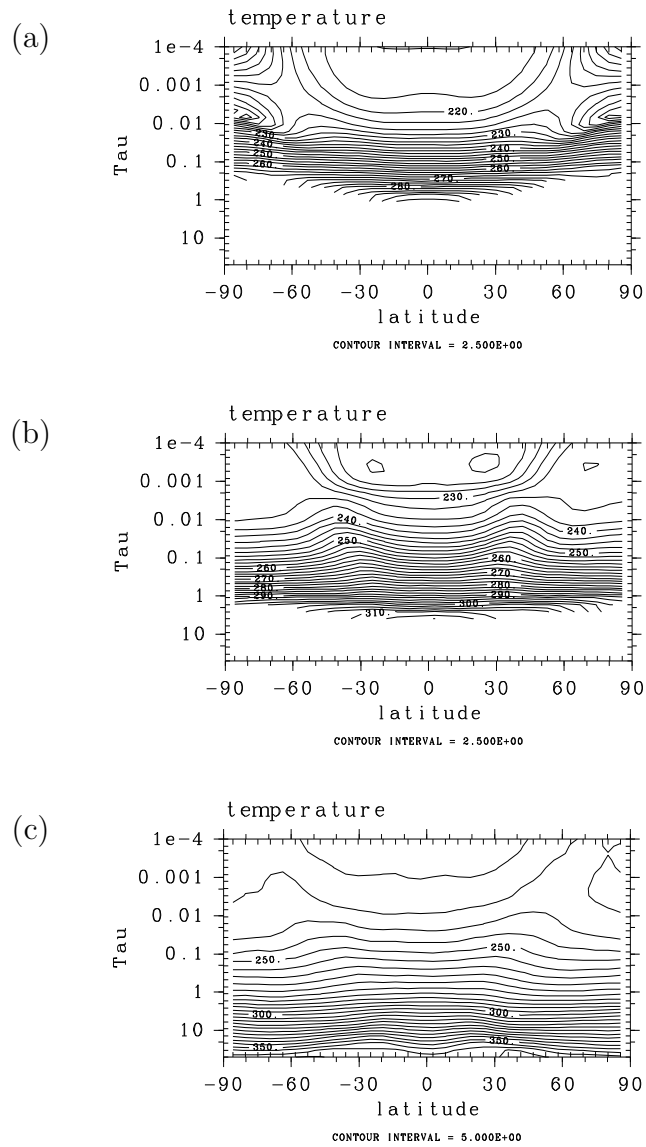


Figure 12: Meridional structure of temperature with the optical depth as the vertical coordinate in the experiments (a) S1380, (b) S1570, and (c) S1800. The areas without data correspond to the regions below the ground surface. The contour intervals are (a) 2.5K, (b) 2.5K, and (c) 5.0K, respectively.

heat budget. This tendency is most notable in the runaway greenhouse state (Fig. 13c), in which the surface radiation flux almost vanishes and most of the incoming heat is supplied to the atmosphere in the form of latent heat flux. Correspondingly, in the profile of precipitation, in addition to the increase at equatorial peak (Figs. 13b,c), there appear new precipitation peaks around latitudes $\pm 60^\circ$. The large amount of latent heat release caused by precipitation in those higher latitudes contributes to the realization of the meridional homogenization of temperature.

The increase of precipitation requires an increase of poleward water vapor transport to compensate for the difference of evaporation and precipitation in the mid- and high latitudes. Fig. 14 shows the distributions of northward transports of dry static energy and latent heat. With the increase of the solar constant, both of the transports increase, but the increase of latent heat transport is more drastic. This is consistent with the result shown in Fig. 13 that the latent heat flux becomes the dominant contributor in the surface heat budget. In the Hadley circulation regions, it is noteworthy that transport by the mean meridional circulation is equatorward in any experiment. This indicates that the mean meridional circulation tends to cause a dry subtropics. The time-dependent eddy transport, however, makes a great contribution to the poleward latent heat transport. Moistening of subtropics is caused by this time dependent eddy contribution. According to detailed observation of horizontal distributions (not shown) of precipitation, humidity and horizontal wind, the time dependent eddy transport is associated with the features that can be regarded as tropical cyclones. In the mid- and high latitudes outside Hadley cells, the poleward latent heat transport is realized by the time-dependent eddy transport (Figs. 14b, d), while in the runaway greenhouse state, the contribution from the mean meridional circulation is not small even in these latitude. (Fig. 14f).

We have to note that, in the runaway greenhouse state, the variation of precipitation is quite large even in the timescale of several days, and correspondingly, the temperature and OLR profiles also change greatly (Fig. 2). Hence, the time mean period of 50 days utilized in drawing those figures may not be enough to smooth the noise to extract proper latitudinal heat transport structure. It is, on the other hand, difficult to use the longer time period for averaging, since in the runaway greenhouse state the thermal structure is continuously changing. For the case of S1800, there remains residual heating in the transport shown in Fig. 14 to cause global warming.

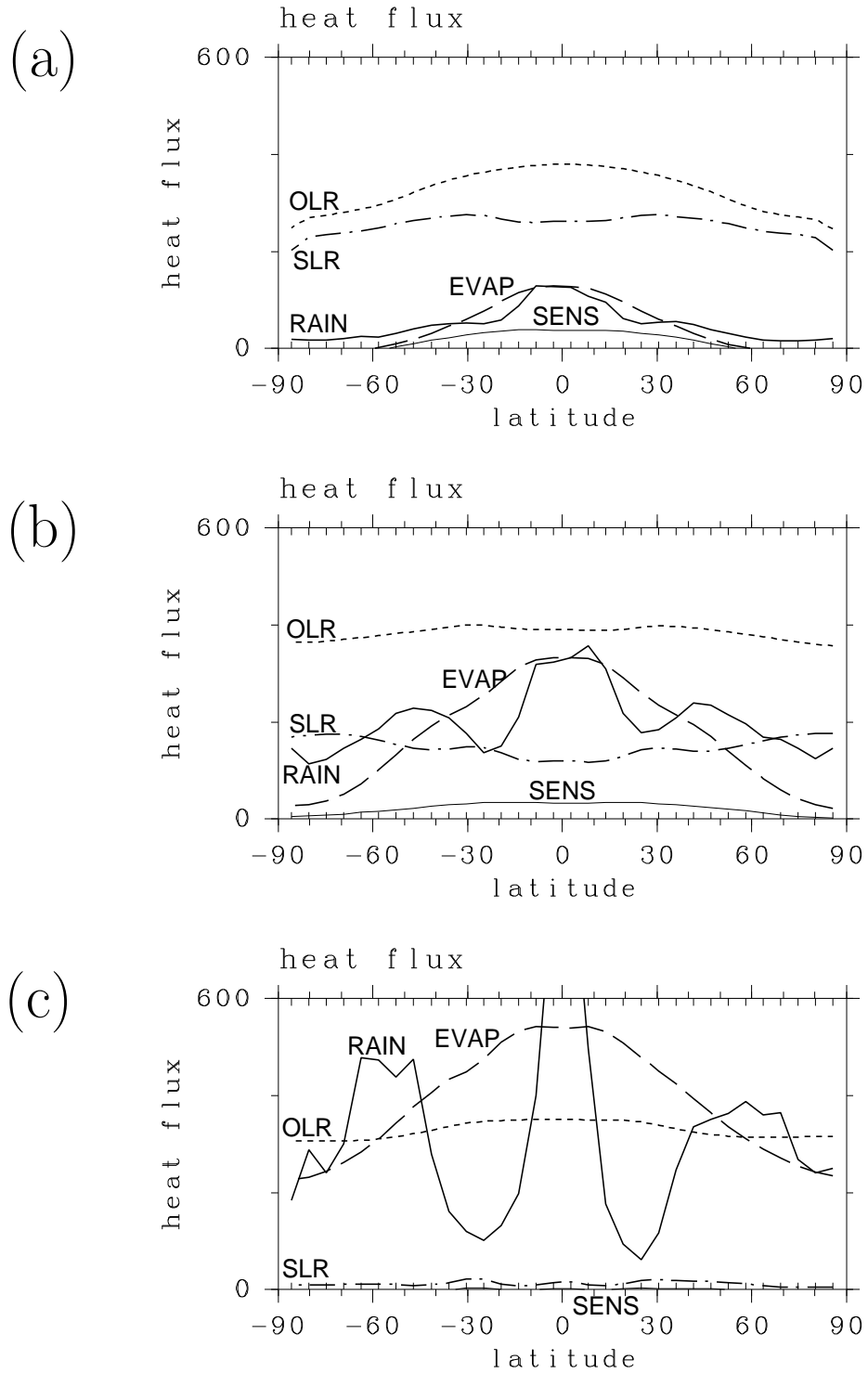


Figure 13: The meridional distributions of vertical energy fluxes in experiments (a) S1380, (b) S1570, and (c) S1800. Thick solid line, dashed line, dotted line, dashed-dotted line, and thin solid line indicate condensation heating (RAIN), evaporation flux (EVAP), OLR, net longwave radiation at the surface (SLR), and sensible heat flux (SENS), respectively. Unit is W m^{-2} . The condensation heating of (c) has its maximum value of 920 W m^{-2} at the equator.

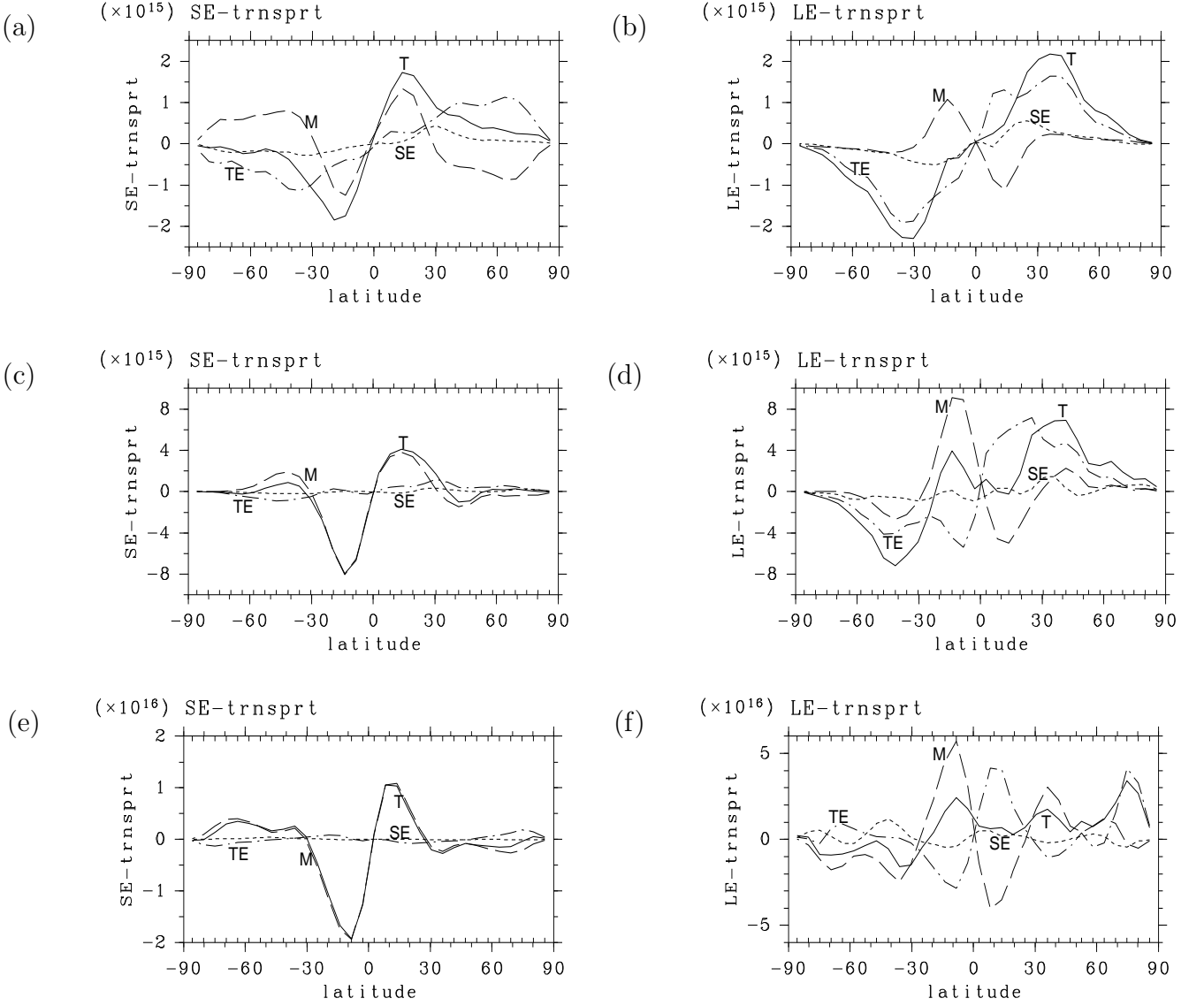


Figure 14: Meridional distributions of latitudinal energy transports. The upper, middle, and lower panels correspond to the experiments S1380, S1570, and S1800, respectively. (a), (c), (e) The sensible heat fluxes; (b), (d), (f) the latent heat fluxes. Unit is W. Thick line is total transport (T), dashed line is zonal and time mean meridional transport (M) $\int_0^1 [\overline{X^\dagger}] [\overline{v^\dagger}] d\sigma$, dotted line is steady eddy transport (SE) $\int_0^1 [\overline{X^* v^*}] d\sigma$, and dashed-dotted line is time dependent eddy transport (TE) $\int_0^1 [\overline{X' v'}] d\sigma$, respectively. Here, X is either dry static energy or latent energy, v is southerly wind velocity, $\overline{\quad}$ and $'$ denote time mean and deviation from the time mean, $[\quad]$ and * denote zonal mean and deviation from the zonal mean, and † denotes the deviation from the vertical mean. According to Masuda (1988), the vertical mean values are subtracted from each quantity in calculating the zonal and time mean meridional transport.

6 Concluding remarks

We have performed a series of numerical experiments using a GCM with a gray atmosphere to investigate a possible three-dimensional counterpart of the runaway greenhouse state defined by NHA92 with a one-dimensional radiative-convective equilibrium model. The experimental results show that, even when the effects of spherical geometry and atmospheric motion are included, there exists an upper limit of OLR at which point the atmosphere with water vapor as an infrared absorber can emit. The value of the upper limit obtained by our experiments is about 400 W m^{-2} , and, correspondingly, the value of the solar constant is 1600 W m^{-2} in the present framework. The experiments also show that when the value of the solar constant exceeds the upper limit of OLR, the atmosphere sets into a thermally runaway state. The upper-limit value is constrained by the vertical structure of the atmosphere in the equatorial region. As the solar constant increases, the temperature distribution at the levels of optical depth around unity becomes uniform in the latitudinal direction, and the values of OLR at all latitudes approach the equatorial limit. The equatorial vertical structure of temperature and radiation can be well described by the one-dimensional radiative-convective equilibrium model of NHA92 by considering the actual value of relative humidity realized in the three-dimensional system. This fact indicates that the thermally runaway state obtained by the three-dimensional calculation is the realization of the runaway greenhouse state defined by NHA92. It is concluded that we can predict the emergence of the runaway greenhouse state by comparing the value of global mean SSR with the upper limit of OLR calculated by the use of the one-dimensional radiative-convective equilibrium model with the relative humidity considered. The condition for the occurrence of runaway greenhouse state in the three-dimensional system is that the global mean value of incident flux, neither the maximum nor the minimum of the latitudinal distribution of incident flux, exceeds the upper limit of OLR.

When the value of the solar constant is increased, the Hadley circulation still exists and is even intensified. Nevertheless, drying in the subtropical regions does not proceed very intensely. Consequently, contrary to our suspicion speculated in Section 1, the increase of subtropical OLR is quite small and the appearance of the runaway greenhouse state has not been prohibited. The reason for the weak drying is that the latent heat transfer by transient eddies is intensified with the increase of solar radiation. Moistening by the eddy mixing in the latitudinal direction, whose contribution is also the issue of subtropical moistening of the real

terrestrial atmosphere (Pierrhumbert, 1998), becomes prominent and counterbalances the equatorward water vapor transfer due to the Hadley circulation. The effect of transient eddies is one of the new findings of this study where an explicit description of atmospheric motion is considered; this cannot be investigated with a one-dimensional model like NHA92. A quantitative assessment of the effects of eddies, however, awaits investigation of the detailed structures and life cycles of transient eddies.

The importance of the contribution of transient eddies suggests that the results of our study—for example, the limit value of incoming solar flux for the emergence of the runaway greenhouse state—may depend on the model resolution. In order to check the resolution dependence of our results, we have performed an experiment with a horizontal resolution T42 at the value of solar constant 1800 W m^{-2} . The results are just as those presented in the proceeding sections; the subtropical drying does not proceed intensely and the runaway greenhouse state emerges (not shown here). It can be concluded that the qualitative features of our results, such as, the emergence of the runaway greenhouse state, do not greatly depend on the model resolution.

From the viewpoint of the evolution of Venusian atmosphere, it has been discussed that a sufficient increase of water vapor mixing ratio in the stratosphere causes water extinction from the planetary surface because of H_2O dissociation and Jeans escape of hydrogen (Hunten, 1973). Stratospheric water vapor mixing ratio larger than 10^{-3} would lead to disappearance of Earth’s oceans in less than about 4 billion years (Kasting, 1988). In our results, the stratospheric values of specific humidity of the experiments S1570 and S1800 are 10^{-4} and 0.1, respectively. Since the escape rate is proportional to the water vapor mixing ratio in the stratosphere, the time scale of the escape of Earth’s ocean is about 40 billion yr for experiment S1570 and 4 million yr for experiment S1800. These estimates suggest that hydrogen escape caused by water vapor dissociation affects the evolution of atmospheric water vapor content only in the runaway greenhouse states. The estimated Jeans escape flux in experiment S1800, however, is not very important for the disappearance of oceans, since the timescale of evaporating oceans by the excess heat flux caused by the runaway greenhouse structure of the experiment S1800 is of the order of a several thousands of years, which is quite smaller than the Jeans escape timescale of hydrogen.

The most troublesome aspect of this study is the vertical filter introduced to enable long-term integration when the value of the solar constant is increased.

Since our aim is to consider the vertical structure of the atmosphere in the framework of NHA92, we keep the assumption made in NHA92 as much as possible, and hence we have assumed that water vapor, whose specific humidity is very small in the upper levels, is the only radiatively active component. This assumption results in tremendous amplification of gravity waves in the upper levels and forces us to introduce the vertical filter. When the vertical filter is applied to the temperature field, upward heat transport caused by the filter contributes to compensate a certain part of the radiative cooling, and consequently, the downward motion of the subtropical branch of Hadley cells reduces to balance only the remaining part of the radiative cooling. Decrease of the intensity of the Hadley circulation causes weakening of the subtropical drying compared with the “correct solution,” which must be realized when the vertical filter is removed. On the other hand, however, we have to recall that water vapor in the subtropics is supplied by the transport due to transient eddy mixing (Fig. 14). There is a possibility that the upward heat transport caused by the vertical temperature filter increases the atmospheric stability, and hence, it reduces the activity of transient eddies. Decrease of the activity of transient eddies causes weakening of the subtropical moistening compared with the correct solution. At the present stage, it is not easy to assess in which way the existence of the vertical temperature filter modifies the subtropical drying and the latitudinal homogenization of OLR compared with the correct solution. In order to consider the results presented by this paper more quantitatively and precisely, we should analyze the vertical propagation properties of disturbances and develop a more physically consistent scheme to damp 2-grid noise. These remain for future investigations.

Finally, we have to note that the calculated values of upper limit of radiation and water vapor content cannot be directly applied to describing the real planetary atmospheres. The physical processes in our model are quite simple; gray radiation scheme without clouds and convective adjustment scheme. The value of the solar constant of the runaway threshold will be changed with the use of different cumulus convection scheme, since the resultant water vapor mixing ratio will be changed. According to the results of Rennó *et al.* (1994), the moist convective adjustment scheme gives the lowest value for the runaway threshold. This result implies that the value of the runaway threshold would become larger, if a more sophisticated cumulus parameterization scheme is adapted. Moreover, the existence of clouds affects the value of the threshold greatly. There are two major competing effects caused by the presence of clouds; cooling effect, which is brought by the reflection of solar radiation, and warming effect, which is brought by the absorption of longwave radiation. It is a controversial and difficult issue

to estimate the qualitative contribution of each effect. According to the results of Kasting (1988), the cooling effect may overcome the warming effect. The value of the runaway threshold would also become larger with the presence of clouds. A sophisticated model is needed to incorporate cloud effect to examine the possible change of the value of the runaway threshold.

A Evaluation of p_s change due to evaporation and condensation

The atmospheric mass varies with the evaporation and condensation (precipitation) of water vapor. We have considered only the total variation of the mass of the vertical column at each grid point and evaluated a correction of surface pressure p_s and specific humidity q after the integration of each time step.

Correction of surface pressure Δp_s for each time step is calculated as follows:

$$\Delta p_s = F_{evap} \frac{g}{L} \Delta t + \hat{p}_s \int S_q^{cond} \Delta t d\sigma \quad (1)$$

The first term on the right hand side describes the water vapor increase by evaporation and the second term describes the water vapor decrease by condensation. The value F_{evap} is the evaporative latent energy flux at the surface, Δt is time step, S_q^{cond} is tendency of specific humidity due to condensation, and \hat{p}_s is surface pressure before correction.

Correction of specific humidity is calculated by use of conservation of mass of water vapor. Mass of water vapor should be conserved through the correction of q as follows,

$$\hat{\rho} \hat{q} = \rho q, \quad (2)$$

where $\hat{\rho}$, \hat{q} are density and specific humidity before correction, and ρ , q are those after correction. From this equation, corrected specific humidity q is

$$q = \frac{\hat{p}_s}{\hat{p}_s + \Delta p_s} \hat{q}. \quad (3)$$

B Vertical filters

In all of the numerical experiments, we have applied a vertical filter to T at all of the vertical grids. The filter utilized is similar to that of Shapiro (1971). Since the original form of the Shapiro filter does not conserve total energy, we have modified the filter in the following way to satisfy energy conservation. This modification is especially important in the experiments where the runaway greenhouse state emerges.

We determine a reference state first. By using the values at half-integer grid points $T_{k+\frac{1}{2}}$, which are calculated in the model for the use of radiation process,

$$T_{B,k} \equiv \frac{T_{k+\frac{1}{2}} + T_{k-\frac{1}{2}}}{2}. \quad (4)$$

The temperature profile is then smoothed toward this reference state. From the bottom ($k = 2$) to the top ($k = 31$), the following scheme is applied.

$$T_{k-1} = \hat{T}_{k-1} + F_T(T_{B,k-1} - T_{k-1}) - \frac{\sum_{k'=k-1}^{k'=k+1} F_T(T_{B,k'} - \hat{T}_k) \Delta p_{k'}}{\sum_{k'=k-1}^{k'=k+1} \Delta p_{k'}}, \quad (5)$$

$$T_k = \hat{T}_k + F_T(T_{B,k} - \hat{T}_k) - \frac{\sum_{k'=k-1}^{k'=k+1} F_T(T_{B,k'} - \hat{T}_k) \Delta p_{k'}}{\sum_{k'=k-1}^{k'=k+1} \Delta p_{k'}}, \quad (6)$$

$$T_{k+1} = \hat{T}_{k+1} + F_T(T_{B,k+1} - \hat{T}_{k+1}) - \frac{\sum_{k'=k-1}^{k'=k+1} F_T(T_{B,k'} - \hat{T}_{k+1}) \Delta p_{k'}}{\sum_{k'=k-1}^{k'=k+1} \Delta p_{k'}}, \quad (7)$$

where \hat{T}_k is the temperature before the filter is applied. The value F_T is a coefficient that describes the intensity of the filter. We utilize $F_T = 0.1$ in our numerical experiments. The third term of the left-hand side in each equation is the correction of the internal energy loss. The energy loss owing to the Shapiro type filter is distributed equally within each three-layer group.

In the cases of $S \geq 1500 \text{ W m}^{-2}$, we have applied a vertical filter also to the horizontal wind field. The filter for the wind field is exactly the same as Shapiro (1971). We have set the intensity parameter of the filter at 0.1.

In our numerical experiments, we have confirmed that these filters give negligible change in the global energy budget.

Acknowledgment

The authors wish to express their thanks to Professor J. F. Kasting and anonymous reviewers for valuable comments on the original manuscript. The numerical integrations were performed at the supercomputer (NEC SX series) of the Center for Global Environmental Research, National Institute for Environmental Studies. The softwares and local computation/information environments were constructed by the use of the resources of GFD-DENNOU CLUB.

References

- Abe, Y., and T. Matsui, 1988: Evolution of an impact-generated H₂O-CO₂ atmosphere and formation of a hot proto-ocean on earth. *J. Atmos. Sci.*, **45**, 3081-3101.
- Akahori, K., and S. Yoden, 1997 : Zonal flow vacillation and bimodality of baroclinic eddy life cycles in a simple global circulation model. *J. Atmos. Sci.*, **54**, 2349-2361.
- Arakawa, A., and M.J. Suarez, 1983: Vertical differencing of the primitive equations in sigma coordinates. *Mon. Wea. Rev.*, **111**, 34-45.
- Gold, T., 1964: Outgassing processes on the moon and venus. *The origin and evolution of atmosphere and oceans*, P.J. Brancazio and A.G.W. Cameron, Eds., Wiley and Sons, 249-256.
- Hayashi, Y.-Y., E. Toyoda, M. Hosaka, S. Takehiro, K. Nakajima, and M. Ishiwatari, 2000: Tropical precipitation patterns in response to a local warm SST area placed at the equator of an aqua planet. *CGER's supercomputer monograph report*, **6**, Center for Global Environmental Research, National Institute for Environmental Studies, 52 pp.
- Horinouchi, T., and S. Yoden, 1997 : Propagation of Waves Exited by Localized Episodic Heating in the Tropics and Their Effect on the Middle Atmosphere: Comparison between two QBO Phases. *J. Meteor. Soc. Japan*, **75**, 641-656.
- Hosaka, M., M. Ishiwatari, S. Takehiro, K. Nakajima, and Y.-Y. Hayashi, 1998: Tropical Precipitation Patterns in the Response to a Local Warm SST Area Placed at the Equator of an Aqua Planet. *J. Meteor. Soc. Japan*, **76**, 289-305.
- Hunten, D. M., 1973: The escape of light gases from planetary atmospheres. *J. Atmos. Sci.*, **30**, 1481-1494.
- Ingersoll, A. P., 1969: The runaway greenhouse: A history of water on Venus. *J. Atmos. Sci.*, **26**, 1191-1198.
- Kasting, J. F., 1988: Runaway and moist greenhouse atmospheres and the evolution of Earth and Venus. *Icarus*, **74**, 472-494.
- Komabayashi, M., 1967: Discrete equilibrium temperatures of a hypothetical planet with the atmosphere and the hydrosphere of one component-two phase system under constant solar radiation. *J. Meteor. Soc. Japan*, **45**, 137-139.

- Louis, J.-F., 1979: A parametric model of vertical eddy fluxes in the atmosphere, *Bound.-Layer Meteor.*, **17**, 187-202.
- Manabe, S., J. Smagorinsky, and R. F. Strickler, 1965: Simulated climatology of a general circulation model with a hydrologic cycle. *Mon. Wea. Rev.*, **93**, 769-798.
- Manzini, E., and K. Hamilton, 1993: Middle atmospheric traveling waves forced by latent had convective heating. *J. Atmos. Sci.*, **50**, 2180-2200.
- Masuda, K., 1988: Meridional heat transport by the atmosphere and the ocean: analysis of FGGE data. *Tellus*, **40**, 265-302.
- Mellor, G., and T. Yamada, 1974: A hierarchy of turbulence closure models for planetary boundary layers. *J. Atmos. Sci.*, **31**, 1791-1806.
- Nakajima, S., Y.-Y. Hayashi, and Y. Abe, 1992: A study on the "Runaway Greenhouse Effect" with a One-dimensional radiative-convective equilibrium model. *J. Atmos. Sci.*, **49**, 2256-2266.
- Numaguti, A., 1992: Numerical experiments on the large scale structure of cumulus activity in the tropics (in Japanese). Ph.D. thesis, University of Tokyo, 205 pp.
- Numaguti, A., 1993: Dynamics and energy balance of the Hadley circulation and the tropical precipitation zones: Significance of the distribution of evaporation. *J. Atmos. Sci.*, **50**, 1874-1887.
- Pierrehumbert, R. T., 1995: Thermostats, Radiator Fins, and the Local Runaway Greenhouse. *J. Atmos. Sci.*, **52**, 1784-1806.
- Pierrehumbert, R. T., 1998: Lateral mixing as a source of subtropical water vapor. *Geophys. Res. Lett.*, **25**, 151-154.
- Plass, 1961: The influence of infrared absorptive molecules on the climate. *Ann. New York Acad. Sci.*, **95**, 61-71.
- Pollack, J. B., 1971: A nongrey calculation of the runaway greenhouse: Implications for Venus' past and present. *Icarus*, **14**, 295-306.
- Rennó, N. O., P. H. Stone, and K. A. Emanuel, 1994: Radiative-convective model with an explicit hydrologic cycle. 2. Sensitivity to large changes in solar forcing. *J. Geophys. Res.*, **99**, 17001-17020.

Satoh, M., 1994: Hadley circulations in radiative-convective equilibrium in an axially symmetric atmosphere. *J. Atmos. Sci.*, **51**, 1947-1968.

Shapiro, R., 1971: The use of linear filtering as a parameterization of atmospheric diffusion. *J. Atmos. Sci.*, **28**, 523-531.

SWAMP project, 1997: AGCM5. GFD-Dennou Club. [Available online at <http://www.gfd-dennou.org/library/agcm5/>]